# A chromatin-wide transition to H4K20 monomethylation impairs genome integrity and programmed DNA rearrangements in the mouse

**Gunnar Schotta,[1,4,5,7] Roopsha Sengupta,[1,4] Stefan Kubicek,[1] Stephen Malin,[1] Monika Kauer,[1] Elsa Callén,[2] Arkady Celeste,[2] Michaela Pagani,[1] Susanne Opravil,[1] Inti A. De La Rosa-Velazquez,[1] Alexsandra Espejo,[3] Mark T. Bedford,[3] André Nussenzweig,[2] Meinrad Busslinger,[1] and Thomas Jenuwein[1,6]**

[1]Research Institute of Molecular Pathology (IMP), The Vienna Biocenter, A-1030 Vienna, Austria; [2]Experimental Immunology Branch, National Cancer Institute, National Institutes of Health, Bethesda, Maryland 20892, USA; [3]University of Texas, M.D. Anderson Cancer Center, Science Park Research Division, Smithville, Texas 79857, USA

**H4K20 methylation is a broad chromatin modification that has been linked with diverse epigenetic functions. Several enzymes target H4K20 methylation, consistent with distinct mono-, di-, and trimethylation states controlling different biological outputs. To analyze the roles of H4K20 methylation states, we generated conditional null alleles for the two *Suv4-20h* histone methyltransferase (HMTase) genes in the mouse. *Suv4-20h*-double-null (dn) mice are perinatally lethal and have lost nearly all H4K20me3 and H4K20me2 states. The genome-wide transition to an H4K20me1 state results in increased sensitivity to damaging stress, since *Suv4-20h*-dn chromatin is less efficient for DNA double-strand break (DSB) repair and prone to chromosomal aberrations. Notably, *Suv4-20h*-dn B cells are defective in immunoglobulin class-switch recombination, and *Suv4-20h*-dn deficiency impairs the stem cell pool of lymphoid progenitors. Thus, conversion to an H4K20me1 state results in compromised chromatin that is insufficient to protect genome integrity and to process a DNA-rearranging differentiation program in the mouse.**

[*Keywords*: H4K20 methylation; Suv4-20h enzymes; DNA repair; genome integrity; B-cell differentiation; class-switch recombination]

Supplemental material is available at http://www.genesdev.org.

Received February 18, 2008; revised version accepted May 30, 2008.

Histone lysine methylation is a central epigenetic modification in eukaryotic chromatin. Five major positions for lysine methylation exist in the histone N termini, each with distinct regulatory functions. The repressive methyl marks H3K9, H3K27, and H4K20 are involved in constitutive heterochromatin formation and gene repression, X inactivation, and Polycomb silencing, and in DNA damage repair, mitotic chromosome condensation, and gene regulation (Allis et al. 2007). Additional complexity arises through the fact that histone methylation can be present in three distinct states (mono, di, or tri), which may have different biological readouts depending on the association with specific binding partners. Although there has been significant insight in histone lysine methylation pathways, we still know very little about how the diverse methylation states affect chromatin biology.

H4K20 methylation is evolutionarily conserved from *Schizosaccharomyces pombe* to man (Lachner et al. 2004). In mammalian cells, H4K20me1 is exclusively induced by the PrSet7/KMT5A histone methyltransferase (HMTase) (Fang et al. 2002; Nishioka et al. 2002), where it has been linked with transcriptional repression (Karachentsev et al. 2005) and X inactivation (Kohlmaier et al. 2004). More recently, genome-wide profiling of H4K20me1 also revealed enrichment of this mark across actively transcribed genes (Papp and Muller 2006; Vakoc et al. 2006). H4K20me1 is very dynamic throughout the cell cycle and becomes highly enriched during S phase (Jorgensen et al. 2007; Tardat et al. 2007; Huen et al. 2008) and on mitotic chromosomes (Rice et al. 2002; Karachent-

**[4]These authors contributed equally to this work.**
**[5]Present address: Munich Center for Integrated Protein Science (CiPS[M]) and Adolf-Butenandt-Institute, Ludwig-Maximilians-Universität München, Schillerstrasse 44, 80336 Munich, Germany.**
**Corresponding authors.**
**[6]E-MAIL jenuwein@imp.univie.ac.at; FAX 43-1-798-7153.**
**[7]E-MAIL Gunnar.Schotta@med.uni-muenchen.de; FAX 49-89-218075425.**
Article is online at http://www.genesdev.org/cgi/doi/10.1101/gad.476008.

sev et al. 2005). Abrogation of H4K20me1 in mitosis results in severe chromosomal segregation defects (Julien and Herr 2004; Houston et al. 2008), and H4K20me1 has been proposed to be an important mark for chromosomal memory (Trojer and Reinberg 2006).

In *S. pombe*, H4K20 methylation by Set9/KMT5 (a PrSet7 ortholog) has been implicated in DNA damage repair (Sanders et al. 2004), although it remained unclear which H4K20 methylation state would operate in this pathway, and H3K79 methylation has also been shown to weaken the DNA damage response (Huyen et al. 2004). Recently, structural studies confirmed association of 53BP1, a DNA damage response factor, with H4K20me2 and, to a lesser extent, also H4K20me1 (Botuyan et al. 2006). However, despite several recent studies to interfere with H4K20 methylation states by RNAi knockdown of H4K20 methylating enzymes in a variety of cell lines (Botuyan et al. 2006; Jorgensen et al. 2007; Tardat et al. 2007; Huen et al. 2008; Yang et al. 2008), the true in vivo functions of H4K20me2 in mammals are largely unknown. In contrast, H4K20me3 is implicated in pericentric heterochromatin formation and is induced by Suv4-20h1/KMT5B and Suv4-20h2/KMT5C enzymes in a sequential pathway that depends on preexisting H3K9me3 marks (Schotta et al. 2004).

While the above examples illustrate the diverse functions of H4K20 methylation at a cellular level, it is not clear whether this modification affects differentiation or, in general, mammalian development. Several HMTases such as Ezh2, G9a, Eset, and Mll2 have been implicated in early mouse development (O'Carroll et al. 2001; Tachibana et al. 2002; Dodge et al. 2004; Glaser et al. 2006). In addition, Ezh2 and H3K27me3 modulate higher-order chromatin structure and thereby regulate V(D)J rearrangement during early B-cell differentiation (Su et al. 2003). Similarly, Suv39h1 and H3K9me3 function in class-switch recombination (CSR), a process required for antibody isotype diversification (Bradley et al. 2006).

To dissect the biological functions of H4K20 methylation during mammalian development and to reduce the complexities of mono-, di-, and trimethylation, we generated conditional mouse knockouts for both *Suv4-20h1* and *Suv4-20h2* genes. *Suv4-20h*-double-null (dn) mice are perinatally lethal and their chromatin has nearly lost all H4K20me3 and H4K20me2, resulting in a genome-wide transition to H4K20me1. This H4K20 monomethylated chromatin displays increased stress sensitivity and defective DNA damage repair, and reveals an important function for the Suv4-20h enzymes in developmentally programmed pathways for DNA rearrangements and during lineage commitment of lymphoid cells.

## Results

### Suv4-20h *mutant mice display perinatal lethality*

Murine Suv4-20h HMTases are encoded by two loci on chromosome 19 (*Suv4-20h1*) and chromosome 7 (*Suv4-20h2*). Whereas *Suv4-20h1* is ubiquitously expressed during embryogenesis and in adult tissues, *Suv4-20h2* mRNAs are much less abundant in the embryo and display restricted expression profile in only some adult tissues (Fig. 1A; Supplemental Fig. S1). Conditional knockout alleles of *Suv4-20h1* and *Suv4-20h2* were engineered using standard technology (Fig. 1A). Germline disruptions of floxed *Suv4-20h1* or of *Suv4-20h2* were subsequently generated by crossing to deleter strains (Mox2-Cre) that induce Cre-mediated recombination of loxP sites in the early embryo.

Intercrosses of *Suv4-20h1*$^{+/-}$ mice produced *Suv4-20h1*$^{-/-}$ pups at sub-Mendelian ratios, indicative of embryonic lethality. Null mutant embryos are born smaller than wild-type littermates and die perinatally a few hours after birth (Fig. 1B), probably due to an alveolar defect in the lungs (data not shown). In contrast, *Suv4-20h2*$^{-/-}$ mice have no apparent defects and develop normally. To exclude functional compensation between *Suv4-20h1* and *Suv4-20h2*, we generated *Suv4-20h*-dn mice by intercrossing *Suv4-20h1*$^{+/-}$; *Suv4-20h2*$^{+/-}$ mice. Similar to *Suv4-20h1*-null mice, *Suv4-20h*-dn mice are born at sub-Mendelian ratios, are smaller, and display perinatal lethality (Fig. 1B). These data indicate an essential function for the Suv4-20h1 enzyme during embryonic and postnatal development.

### *A genome-wide transition to H4K20 monomethylation in* Suv4-20h-*dn mouse embryonic fibroblasts (MEFs)*

In order to address the effect of Suv4-20h abrogation on H4K20 methylation, we first analyzed all three H4K20 methylation states in wild-type and *Suv4-20h*-null primary MEFs (pMEFs) by indirect immunofluorescence (IF). In wild-type cells, H4K20me1 shows a broad nuclear staining with enrichment at the inactive X chromosome (Xi) in female cells (Fig. 2A, arrows). H4K20me2 also displays a broad, yet more speckled nuclear staining without an apparent subnuclear enrichment; however, H4K20me2 IF signals may be under-represented due to reduced accessibility of the epitope (see the Material and Methods). As previously reported, H4K20me3 accumulates at pericentric heterochromatin (Fig. 2A; Schotta et al. 2004). In *Suv4-20h1*-null pMEFs, H4K20me2 is reduced, whereas H4K20me3 appears unaltered. In contrast, *Suv4-20h2*-null cells show selective loss of H4K20me3, but maintain H4K20me2. Importantly, in *Suv4-20h*-dn pMEFs both H4K20me2 and H4K20me3 are nearly lost, with a concomitant increase in H4K20me1 that now becomes detectable at pericentric heterochromatin (Fig. 2A).

To quantify the observed changes in H4K20 methylation patterns, we next used mass-spectrometry of bulk histones (see the Material and Methods). In wild-type pMEFs, H4K20me2 is the most abundant histone lysine methyl mark and is present in around 85% of all histone H4 molecules (Fig. 2B). H4K20me1 (~5%) and H4K20me3 (~10%) are much less frequent. In *Suv4-20h1*-null cells, H4K20me2 is reduced to ~60%, with a concomitant increase in H4K20me1 (~30%). In agreement with the IF data, *Suv4-20h2*-null cells selectively lose H4K20me3. Notably, in *Suv4-20h*-dn pMEFs, there is a pronounced

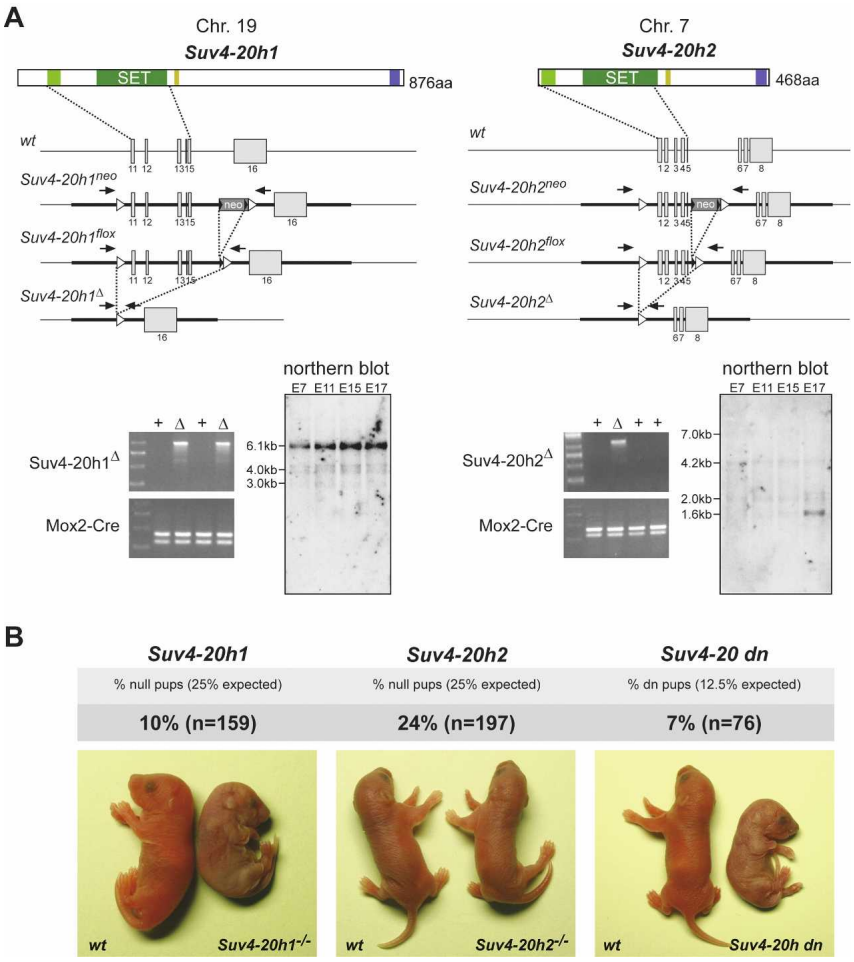


**Figure 1.** *Suv4-20h*-dn mice display perinatal lethality. (*A*) Generation of *Suv4-20h1* and *Suv4-20h2* conditional knockouts. For both genes, targeting constructs (thick black bar) were generated that contain loxP sites in introns flanking the SET domain coding region. To remove the FRT-flanked neomycin resistance cassette, *Suv4-20h*$^{neo/+}$ mice were crossed with Flp recombinase expressing mice. Mox2-Cre was used for germline deletion (confirmed by PCR, *bottom* panel). Northern blot analysis of four embryonic stages indicates ubiquitous expression of *Suv4-20h1* (*left* panel) and only low abundance of *Suv4-20h2* (*right* panel). (*B*) Homozygous mutant mice were generated by intercrossing *Suv4-20h1*$^{+/-}$ or *Suv4-20h2*$^{+/-}$. To generate *Suv4-20h*-dn mice, doubly heterozygous *Suv4-20h1*$^{+/-}$; *Suv4-20h2*$^{+/-}$ mice were intercrossed. *Suv4-20h1*-null and *Suv4-20h*-dn embryos were born at sub-Mendelian ratios, are smaller than their littermates, and die perinatally.

conversion of H4K20 methylation states, such that H4K20me2 and H4K20me3 are almost lost and ~90% of the H4 molecules now carry the H4K20me1 mark (Fig. 2B). These data suggest that Suv4-20h1 is largely responsible for H4K20me2, whereas Suv4-20h2 primarily regulates H4K20me3. In contrast to isolated cell cultures—such as, e.g., pMEFs—H4K20me3 is not fully abrogated in embryonic tissues of *Suv4-20h2*-null mice (Supplemental Fig. S2), indicating partial compensation by Suv4-20h1 or by a different HMTase.

We also examined acetylation and methylation states of H3K9, H3K14, H3K23, H3K27, H3K36, and H4 by a similar mass-spec analysis comparing wild-type and *Suv4-20h*-dn pMEFs. No significant changes in any of these modifications could be detected (Supplemental Fig. S3). We conclude that the Suv4-20h HMTases are the major enzymes to induce H4K20me2 and H4K20me3 states in mammalian chromatin, and that removal of both enzymes results in a genome-wide transition to H4K20me1.

### Suv4-20h-*dn pMEFs display proliferation and cell cycle defects*

To examine the biological role of *Suv4-20h*-dn deficiency, we first compared proliferation rates and cell cycle progression of wild-type and *Suv4-20h*-dn pMEFs. Under normal culture conditions, wild-type cells start entering crisis after more than five passages. *Suv4-20h*-dn cells show reduced proliferation rates and plateau much earlier (Fig. 3A). FACS analysis for DNA content revealed broader G1 and G2 peaks in *Suv4-20h*-dn cells at higher passage numbers (Fig. 3B). *Suv4-20h*-dn cells do not appear to enter aberrant apoptosis, because no significant sub-G1 peak is detected. However, BrdU labeling of wild-type and *Suv4-20h*-dn pMEFs indicates higher percentages of noncycling cells in early passage *Suv4-20h*-dn populations (Supplemental Fig. 4A).

A more detailed analysis of cell cycle stages after BrdU pulse-labeling reveals reduction of S-phase cells with a concomitant increase of G1-phase cells, indicating a partial block in G1–S transition (Fig. 3C). To address whether G1–S transition is indeed delayed in *Suv4-20h*-dn cells, we next synchronized early passage pMEFs by serum starvation and monitored S-phase entry after serum addition. There is a significant delay for *Suv4-20h*-dn cells in S-phase entry as compared with wild-type cells (Fig. 3D). Together, these data indicate proliferation defects in *Suv4-20h*-dn cells that would be consistent with impaired cell cycle progression and higher sensitivity to stress-induced damage (Kodama et al. 2001).

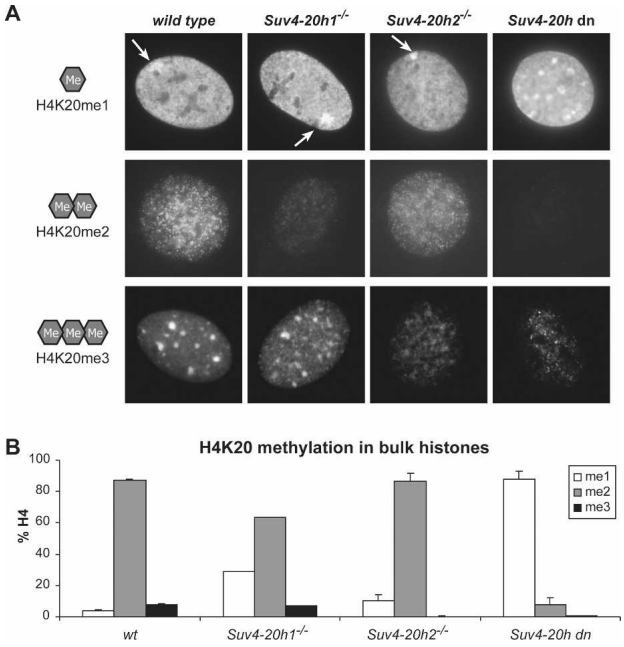


**Figure 2**. A genome-wide transition to H4K20me1 in *Suv4-20h*-dn pMEFs. (*A*) In wild-type pMEFs, H4K20me1 and H4K20me2 are broadly nuclear, H4K20me3 is focally enriched at pericentric heterochromatin. In female cells, H4K20me1 shows enrichment at the inactive X chromosome (arrows). In *Suv4-20h1*$^{-/-}$ cells, H4K20me2 is reduced, whereas *Suv4-20h2*$^{-/-}$ cells show loss of pericentric H4K20me3. In *Suv4-20h*-dn pMEFs, both H4K20me2 and H4K20me3 are strongly reduced with a concomitant increase in H4K20me1. (*B*) Overall H4K20 methylation levels were quantified by mass-spec of bulk histones. In wild-type cells, H4K20me2 is the most prominent mark present in ~85% of all histone H4 molecules. In *Suv4-20h*-dn cells H4K20me2 and H4K20me3 are markedly reduced resulting in a genome-wide switch to H4K20me1.

We next asked whether proliferation defects in *Suv4-20h*-dn pMEFs could be due to defects in DNA damage response. We first tested the G2–M checkpoint that prevents entry into mitosis when DNA damage is not completely repaired (Sancar et al. 2004). DNA double-strand breaks (DSB) were induced with varying doses of ionizing radiation (IR). Both wild-type and *Suv4-20h*-dn pMEFs show dose-dependent reduction in the number of mitotic cells, indicating that the G2–M checkpoint is functional (Supplemental Fig. S4B). We then analyzed chromosomal abnormalities in mitotic spreads of wild-type and *Suv4-20h*-dn pMEFs that would be indicative of defective DNA damage repair. Exponentially growing pMEFs were treated with 2 Gy IR and left for 1 h to allow for DSB repair. Following this, cells were arrested in mitosis by nocodazole treatment and metaphase spreads were prepared. Wild-type cells can efficiently repair DNA damage, as only a few chromosomal gaps are observed in the metaphase spreads (Fig. 3E). In contrast, the number of aberrant chromosomes displaying gaps and breaks is modestly increased in *Suv4-20h*-dn pMEFs (Fig. 3E,F). In a second series of experiments, cell cycle arrest was blocked with the ATM/ATR inhibitor caffeine 1 h post-treatment. These conditions allow cells with DNA damage to proceed to metaphase, resulting in a higher percentage of chromatid breaks (Fig. 3F).

### *Increased DNA damage sensitivity of H4K20me1 chromatin*

To address how the genome-wide removal of H4K20me2 and H4K20me3 would impair proliferation, genomic in-

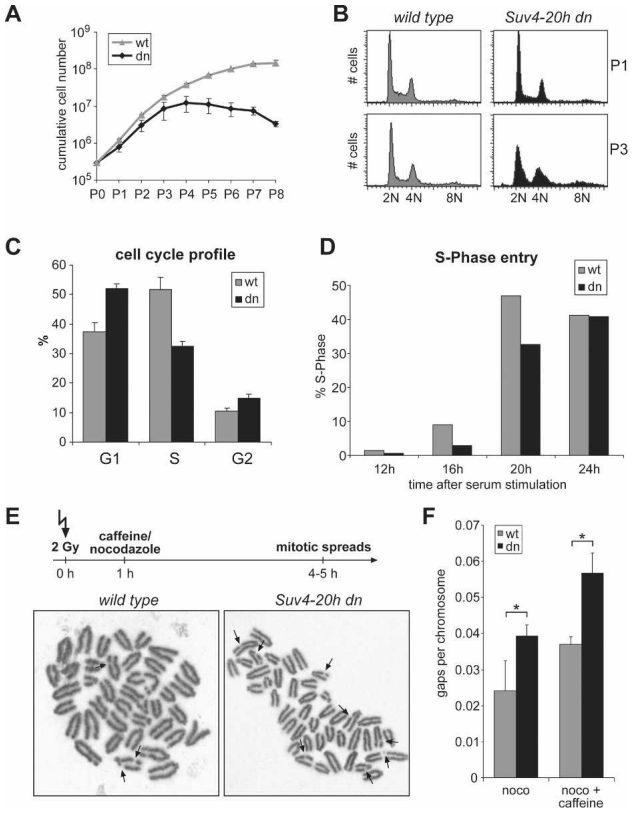


**Figure 3**. *Suv4-20h*-dn pMEFs display proliferation and cell cycle defects. (*A*) Proliferation of wild-type and *Suv4-20h*-dn pMEFs was measured by counting cell numbers of serially passaged cells. *Suv4-20h*-dn cells show less cumulative growth and plateau earlier than wild-type cells. (*B*) DNA content of wild-type and *Suv4-20h*-dn pMEFs was determined by FACS analysis of PI-labeled early (P1) and later passage (P3) cells. *Suv4-20h*-dn cells display broader G1 and G2 peaks at passage 3. (*C*) Exponentially growing pMEFs (P1) were pulse-labeled with BrdU and percentages of G1-, S-, and G2-phase cells were determined by FACS analysis. (*D*) Early passage pMEFs were synchronized in G0 by serum deprivation. Re-entry into S Phase was measured by BrdU pulse-labeling after serum add-back (one representative data-set of three independent experiments is shown). (*E*) Logarithmically growing pMEFs were treated with 2Gy IR. One hour post-IR treatment, either nocodazole or caffeine plus nocodazole were added to the medium, and 4–5 hours later mitotic spreads were prepared. Mitotic chromosomes of *Suv4-20h*-dn cells show more chromosomal gaps (arrows) than wild-type cells. (*F*) Summary of chromosomal gaps and breaks in >100 mitotic chromosome preparations. Asterisks indicate statistically significant differences (Wilcoxon-Mann-Whitney test, $P < 0.05$).

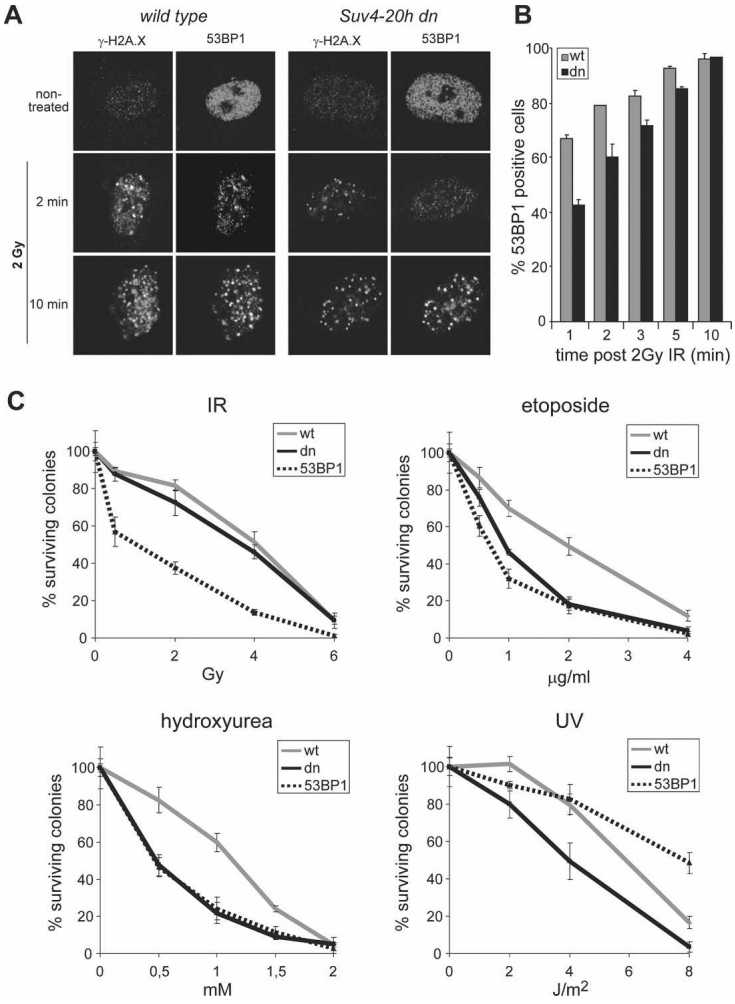


**Figure 4.** Increased DNA damage sensitivity in H4K20me1 chromatin. (*A*) Wild-type and *Suv4-20h*-dn pMEFs were treated with 2 Gy IR, fixed after different time-points (1–10 min), and stained with antibodies against γH2A.X and 53BP1. (*B*) Numbers of 53BP1-positive cells (more than one focus per cell) were counted at different time-points post-treatment with 2 Gy IR. At early time-points (2 min), *Suv4-20h*-dn cells display reduced focal enrichment of 53BP1. At later time points (10 min), wild-type and *Suv4-20h*-dn cells show comparable 53BP1 foci. (*C*) Colony formation assays to assess sensitivity of *Suv4-20h*-dn and *53BP1*-null cells to various types of DNA damage. Wild-type, *53BP1*-null, and *Suv4-20h*-dn MEFs were plated at low density and treated with indicated doses of IR, etoposide, hydroxyurea, and UV. The percentage of surviving colonies relative to the nontreated samples is plotted.

tegrity, and DNA damage repair, we analyzed downstream read-outs. Earlier work in *S. pombe* (Sanders et al. 2004; Du et al. 2006) and mammalian cells (Botuyan et al. 2006) suggested that 53BP1, a protein involved in DNA damage repair, binds to H4K20 methylation. Also, Dot1-mediated methylation of H3K79 has been shown to weaken the DNA damage response and could facilitate 53BP1 recruitment (Huyen et al. 2004; Wysocki et al. 2005). Although instructive, these studies did not address 53BP1 binding to a physiological template. A nucleosomal context for 53BP1 interaction is particularly important for the H4K20 position, since Suv4-20h HMTases specifically methylate nucleosomes, but show only little activity toward histone peptides (Schotta et al. 2004). Therefore, we used Suv4-20h enzymes to generate in vitro methylated nucleosomes, which serve as a strong binding substrate for 53BP1 (Supplemental Fig. S5).

The conserved checkpoint protein 53BP1 localizes to DSBs within minutes post-damage and participates in DNA damage repair (Schultz et al. 2000; Ward et al. 2003). To examine whether H4K20me1 chromatin may be compromised in 53BP1-mediated DNA damage response, we exposed wild-type and *Suv4-20h*-dn pMEFs to 2 Gy of IR and then monitored formation of γH2A.X and 53BP1 foci by IF. Nontreated cells are largely negative for γH2A.X and show dispersed 53BP1 staining. However, as early as 1–2 min post-damage, most wild-type cells have formed small 53BP1 foci that overlap with γH2A.X, whereas *Suv4-20h*-dn cells only display reduced focal enrichment of 53BP1 (Fig. 4A). At later time points (10 min), nearly all wild-type and *Suv4-20h*-dn cells show comparable γH2A.X and 53BP1 foci (Fig. 4A). We quantified this differential 53BP1 recruitment, which indicates that only at very early time points after damage (<5 min), there are reduced numbers of 53BP1-positive *Suv4-20h*-dn cells (Fig. 4B).

We next examined DNA damage sensitivity by colony formation assays (see the Materials and Methods) and by comparing *Suv4-20h*-dn with *53BP1*-null MEFs (Ward et al. 2003). *53BP1*-null MEFs show pronounced sensitivity toward IR-induced DNA damage, which is not reflected in *Suv4-20h*-dn cells (Fig. 4C, top left panel). This result is in agreement with data from *S. pombe*, where cells remain insensitive to IR despite impaired recruitment of Crb2 (a 53BP1 ortholog) to DSBs, due to loss of H4K20 methylation or mutations in the Crb2 tudor domain (Du et al. 2006), suggesting that binding of 53BP1 to

H4K20me2 is not critical for cell survival after IR damage. We then extended our analysis to other DNA-damaging agents, such as etoposide, a specific inhibitor of topoisomerase II, and to the replication inhibitor hydroxyurea. Under these stress conditions, *Suv4-20h*-dn cells display a very similar increase in damage sensitivity as compared with *53BP1*-null MEFs (Fig. 4C). In contrast, upon UV-induced damage, *Suv4-20h*-dn cells are more sensitive than *53BP1*-null MEFs (Fig. 4C, bottom right panel). Together, these data indicate partially overlapping functions for the Suv4-20h enzymes and 53BP1 in certain DNA damage response pathways, but also reveal selective roles for H4K20 methylation that appear to be independent of 53BP1.

### *Conditional deletion of the* Suv4-20h *genes in the hematopoietic system*

The impairment of the DNA damage response suggests that *Suv4-20h* deficiency may also affect lineage programs in the mouse, where DSB-mediated DNA rearrangements dictate transitions between progenitor and fully differentiated cells. Paradigms for these processes are B and T cells of the hematopoietic system that rearrange variable regions of antigen receptor loci [V(D)J recombination] and constant regions of immunoglobulin genes (CSR), thereby allowing antibody diversity (Dudley et al. 2005).

To address a possible role for the Suv4-20h enzymes in these processes, we inactivated Suv4-20h function by crossing compound *Suv4-20h1*$^{f/f}$, *Suv4-20h2*$^{-/-}$ mice to a deleter strain (vav Cre) that expresses the Cre recombinase in hematopoietic stem cells (HSCs) and should, therefore, delete Suv4-20h enzymes in all cells of the hematopoietic system. *Suv4-20h*-dn$^{vav}$ mice are viable and do not show any gross abnormalities. RT–PCR demonstrates efficient deletion of *Suv-20h1*$^{f/f}$, since no *Suv4-20h1* (and no *Suv4-20h2*) transcripts can be detected in *Suv4-20h*-dn$^{vav}$ CD19$^{+}$ B cells (Supplemental Fig. S6A). In addition, we analyzed H4K20 methylation states in wild-type and *Suv4-20h*-dn$^{vav}$ CD19$^{+}$ B cells by mass-spec of bulk histones. Deletion of both Suv4-20h enzymes in B cells also leads to a genome-wide conversion to H4K20me1 chromatin (Supplemental Fig. S6B).

*V(D)J* recombination assembles the variable regions of immunoglobulin (*Ig*) genes from discontinuous variable (*V*), diversity (*D*), and joining (*J*) gene segments in pro-B cells by a sequence-specific Rag1 and Rag2-mediated recombination mechanism (Dudley et al. 2005).We isolated genomic DNA from sorted wild-type, *Suv4-20h*-dn$^{vav}$, and *Pax5*$^{-/-}$ pro-B cells and quantified successful V(D)J rearrangements by $V_H$ segment-specific PCR. In contrast to the Pax5 mutant control, which has impaired joining of the more distal $V_H$ segments (Fuxa et al. 2004), *Suv4-20h*-dn$^{vav}$ pro-B cells do not show apparent defects in V(D)J recombination (Supplemental Fig. S7). We also examined V(D)J recombination of the TCRβ locus in wild-type and *Suv4-20h*-dn$^{vav}$ pro-T cells and could not detect any gross abnormalities (Supplemental Fig. S8). We conclude that Suv4-20h enzymes have no primary function in V(D)J recombination of both pro-B and pro-T cells.

### Suv4-20h-*dn B cells are defective in CSR*

CSR in the immunoglobulin heavy chain (*IgH*) locus is a process that changes the antibody effector function by

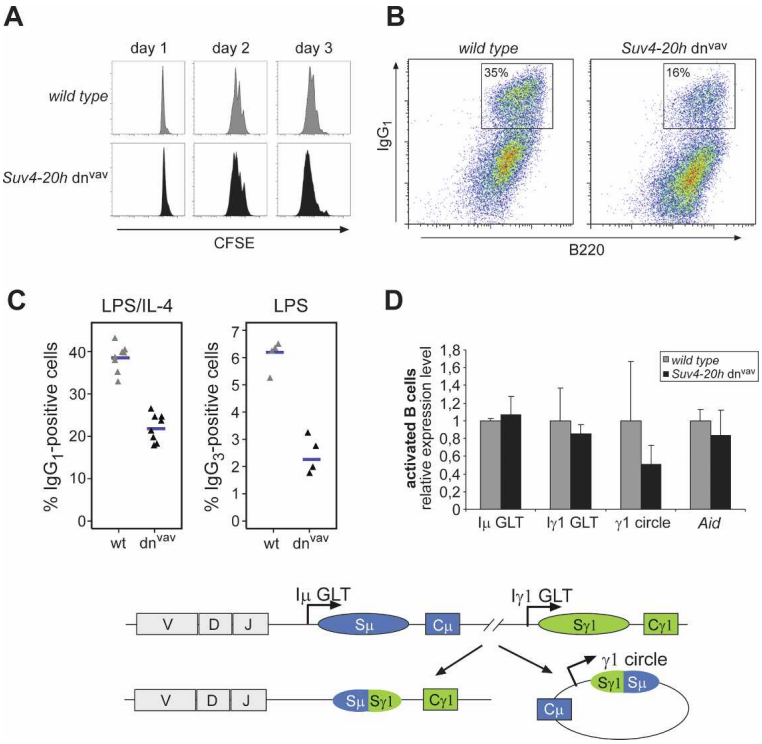


**Figure 5.** *Suv4-20h*-dn B cells are defective in CSR. (*A*) Wild-type and *Suv4-20h*-dn$^{vav}$ B cells were labeled with CFSE and stimulated with LPS/IL-4. Comparable proliferation rates of wild-type and Suv4-20h-dn$^{vav}$ B cells are indicated by a similar decrease of CFSE intensity. (*B*) Number of $IgG_1$-expressing B cells was determined 4 d after stimulation with LPS/IL-4 by FACS analysis. (*C*) Box plot representations for the percentage of switched B cells from eight ($IgG_1$) or four ($IgG_3$) independent CSR experiments. (*D*) Relative expression levels of GLTs, circle transcript, and *Aid* were analyzed by quantitative RT–PCR 4 d after stimulation with LPS/IL-4 (normalized to the average of *Gapdh*, *HPRT*, and *tubulin* expression levels). The *bottom* diagram shows a schematic representation of CSR between Sμ and Sγ1 constant regions in the *IgH* locus.

replacing the default constant region (Cμ) of the antibody gene with a different constant region. This process is not sequence specific and involves the generation of DSBs in highly repetitive switch (S) regions, which precede every individual constant region (see Fig. 5, bottom diagram). These DSBs are processed by the DNA damage machinery (Dudley et al. 2005). Mature B cells primarily generate the IgM isotype [from the V(D)J most-proximal Cμ region] and, upon specific antigen stimulation with LPS/IL-4, predominantly switch to the $IgG_1$ isotype.

To examine whether CSR is impaired in *Suv4-20h*-dn$^{vav}$ mice, we stimulated B220$^+$ splenic B cells with LPS/IL-4 to induce switching from Cμ to C$\gamma_1$. Comparable proliferation rates over a 3-d period between wild-type and mutant samples were confirmed by CFSE fluorescent labeling of B220$^+$-sorted B cells (Fig. 5A). Whereas 35% of wild-type B cells showed expression of $IgG_1$, only 16% of *Suv4-20h*-dn$^{vav}$ B cells were $IgG_1$-positive (Fig. 5B). The experiment was repeated with B-cell preparations from eight independent *Suv4-20h*-dn$^{vav}$ mice, consistently demonstrating reduced efficiency in CSR to $IgG_1$ (Fig. 5C). We next examined whether CSR to other isotypes may also be impaired by stimulating B220$^+$ B cells with LPS only to induce switching to $IgG_3$. In wild-type B cells we observed ~6% $IgG_3$-positive cells, whereas in *Suv4-20h*-dn$^{vav}$ B cells, this number is decreased to 2%–3% (Fig. 5C).

Efficient CSR correlates with the expression of so-called germline transcripts (GLTs) initiated at the promoters upstream of the switch regions (see bottom diagram in Fig. 5), which are proposed to make the chromatin domain accessible for the induction of DSBs (Dudley et al. 2005). We therefore measured the abundance of Iμ and Iγ1 GLTs in wild-type versus *Suv4-20h*-dn$^{vav}$ B cells by real-time RT–PCR. As shown in Figure 5D, Iμ and Iγ1 GLTs are expressed at similar levels. A byproduct of productive CSR is the generation of a looped-out circular DNA fragment that contains joined segments of the Sμ and Sγ1 switch regions that are preceded by an intronic promoter. Joined SμSγ1 transcripts from this circular DNA only occur after productive CSR, and their abundance is directly proportional to the frequency of productive switching events (Dudley et al. 2005). We quantified these SμSγ1 circle transcripts by real-time RT–PCR, which are significantly reduced in *Suv4-20h*-dn$^{vav}$ B cells (Fig. 5D).

### *Altered chromatin structure and increased chromosomal aberrations in* Suv4-20h-*dn$^{vav}$ B cells*

Next, we addressed whether transcriptional changes in *Suv4-20h*-dn$^{vav}$ B cells could be responsible for defective CSR. The activation-induced deaminase (Aid), which targets switch regions and generates a DNA damage signal by deamination of cytidine nucleotides is such an essential factor, since CSR is abrogated in *Aid*-null mice (Muramatsu et al. 2000). Real-time RT–PCR analysis revealed no significant alteration in *Aid* expression levels in activated B cells (see Fig. 5D). We then performed global expression profiling using Affymetrix tiling arrays to analyze possible changes in gene expression between wild-type versus *Suv4-20h*-dn$^{vav}$ B cells before and after antigen stimulation. These, and similar analyses in embryonic stem (ES) cells, revealed that out of ~35,000 ESTs, <150 genes were either slightly up- or down-regulated in *Suv4-20h*-dn$^{vav}$ B cells (Supplemental Fig. S9). None of the affected genes is reported to be involved in CSR or DNA damage control (Supplemental Tables S1–S3). From these data we conclude that Suv4-20h deficiency has only a minor impact on general transcriptional regulation. By comparison, abrogation of the transcription factor Pax5 in B cells results in ~300 genes that are aberrantly regulated with much more significant differences in their expression levels (Delogu et al. 2006; Schebesta et al. 2007).

The defects in CSR could be caused by alterations in the chromatin structure at the IgH locus. Therefore, we analyzed major histone lysine methylation marks at the Igμ and Igγ1 promoter and at their associated switch regions (Fig. 6A, top diagram) in wild-type versus *Suv4-20h*-dn$^{vav}$ B cells by directed chromatin immunoprecipitation (ChIP). In resting wild-type B cells, the Igμ promoter is active, whereas the Igγ1 region is silent (Dudley et al. 2005). In agreement, we detect significant enrichment for H3K4me3 across the Igμ, but not the Igγ1 region, which instead is decorated by the repressive H3K27me3 mark (Fig. 6A, bottom left panels). For H3K9me3 and H4K20me3, there are only low-level enrichments with both the Igμ and Igγ1 probes. Importantly, H4K20me1 is high across Igμ, but only with residual signals across Igγ1 (Fig. 6A, top left panel). We could not examine H4K20me2, since several attempts with distinct H4K20me2 antibodies failed to indicate reliable enrichment at the IgH locus and also at other chromosomal regions (data not shown).

Upon activation of wild-type B cells, this chromatin profile is altered by three major changes, such that H3K4me3 is now present across Igγ1 (with a concomitant decrease for H3K27me3), H4K20me1 signals at Igμ are reduced and H4K20me3 is elevated with three out of five Igγ1 probes (Fig. 6A, right panels). Importantly, in both resting and activated *Suv4-20h*-dn$^{vav}$ B cells, the Igμ and Igγ1 chromatin structure is locked with high H4K20me1 marks, thereby impairing the downshift for H4K20me1 at Igμ and reducing H3K4me3 accumulation at Igγ1 (Fig. 6A, both panels).

The aberrantly high H4K20me1 levels across the Igγ1 region in both resting and activated *Suv4-20h*-dn$^{vav}$ B cells could affect processing of Aid-induced DSBs also beyond impaired CSR. Therefore, we examined IgH-associated chromosomal abnormalities in activated wild-type and *Suv4-20h*-dn$^{vav}$ B cells by chromosome painting and IgH-telomere FISH analysis (Callen et al. 2007). Isolated splenic B cells were stimulated with LPS/IL-4 for 3 d, and mitotic chromosome spreads were then prepared. As shown in Figure 6B, left panel, the IgH locus is located close to the telomeric region of chromosome 12. Notably, we detect IgH-associated translocations (T12;12) and deletions (Del12) in mitotic spreads from six independently isolated *Suv4-20h*-dn$^{vav}$ B-cell samples (Fig. 6B). To determine whether IgH-specific chromosomal instabili-

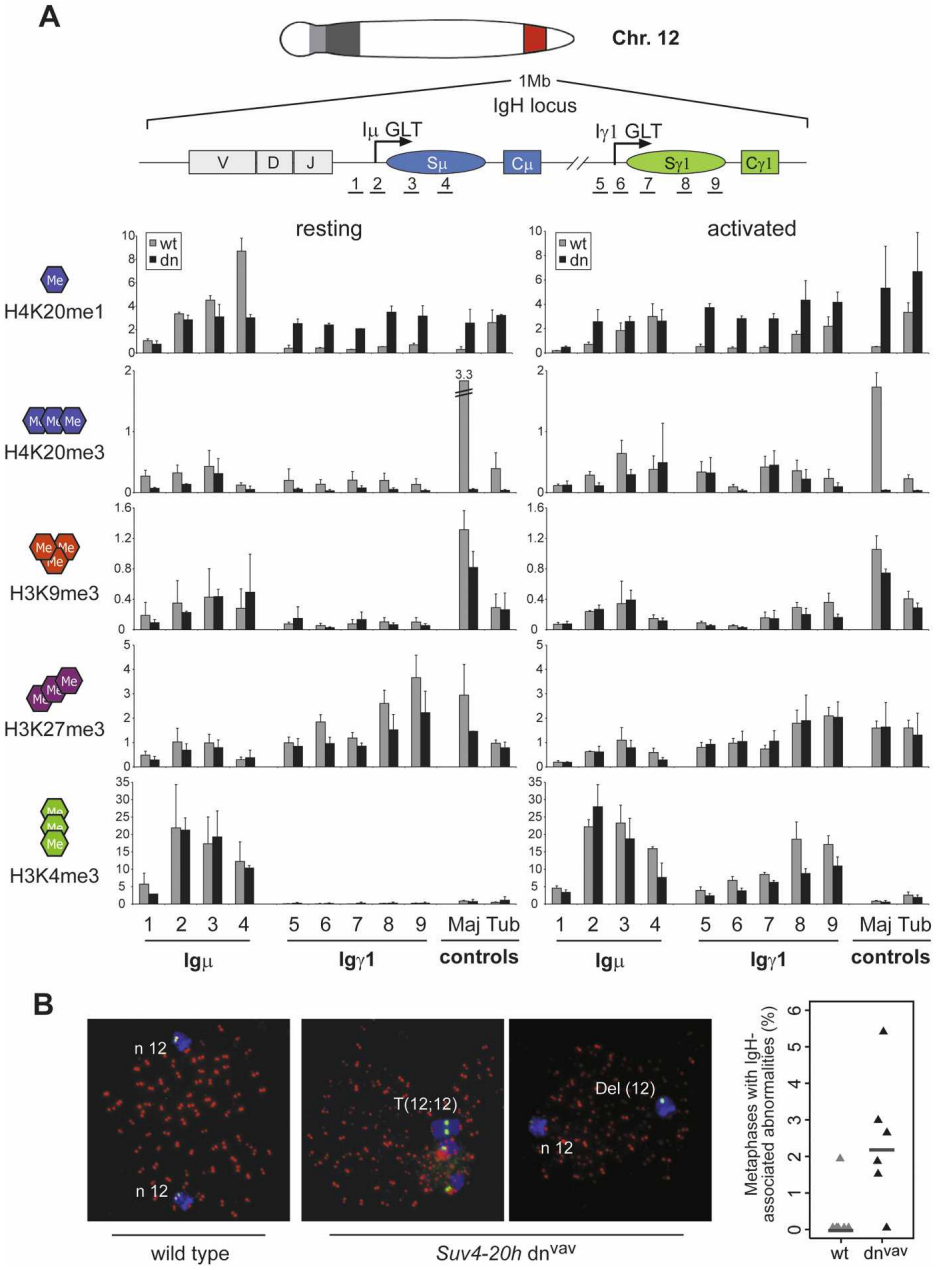


**Figure 6.** Altered chromatin structure and increased chromosomal aberrations in *Suv4-20h*-dn$^{vav}$ B cells. (*A*) Histone modifications at the Igμ and Igγ1 promoter and their associated switch regions of the IgH locus were determined by directed ChIP in resting and activated B cells. The *top* diagram indicates the approximate positions of the primer pairs. Histone modifications for major satellite repeats and tubulin served as controls. (*B*) IgH-associated chromosomal abnormalities were analyzed in metaphase spreads of activated wild-type and *Suv4-20h*-dn$^{vav}$ B cells using chromosome painting in combination with IgH-FISH. In wild-type B cells, the IgH locus (green dots) is located on chromosome 12 (blue), proximal to the telomeres (red dots). Elevated levels of IgH-associated translocations (T) or Deletions (Del) were observed in *Suv4-20h*-dn$^{vav}$ B cells. The box plot shows percentages of IgH-associated abnormalities in six independent wild-type (362 spreads) and *Suv4-20h*-dn$^{vav}$ (379 spreads) B-cell preparations.

ties are dependent on impaired CSR, we stimulated B cells from wild-type and *Suv4-20h*-dn$^{vav}$ mice with anti-RP105, which induces proliferation, but not class switching (Callen et al. 2007). In neither wild-type ($n$ = 80) nor *Suv4-20h*-dn$^{vav}$ ($n$ = 80) mitotic spreads could we identify IgH-associated chromosomal aberrations (Supplemental Fig. S10).

### *Suv4-20h-dn deficiency impairs the stem cell potential for lymphoid cells*

The Suv4-20h enzymes are expressed throughout distinct stages of B-cell development and down-regulated upon B-cell activation. This expression profile is similar to the B-cell-specific transcription factors NFκB and

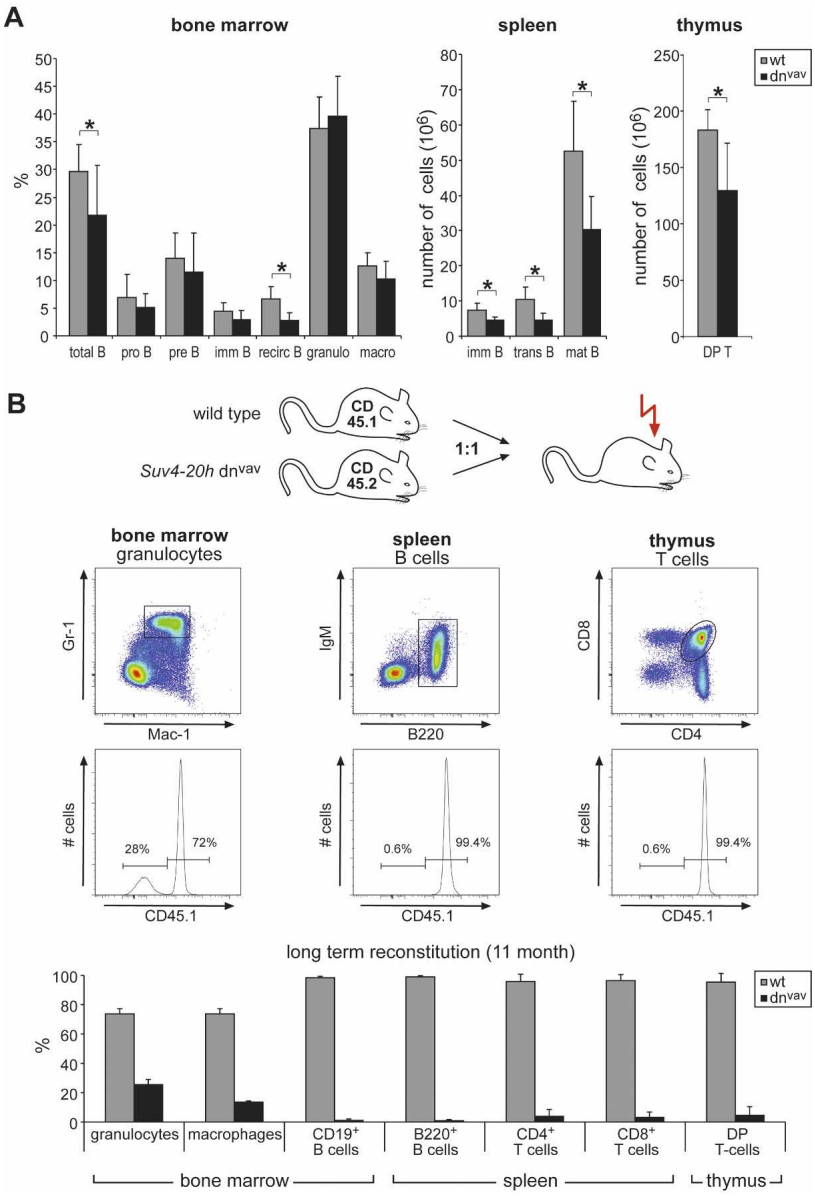


**Figure 7.** *Suv4-20h* deficiency impairs the stem cell potential for lymphoid cells. (*A*) Bone marrow, spleen, and thymus of eight independent 2-mo-old wild-type and *Suv4-20h*-dn$^{vav}$ mice were analyzed by FACS for different B-cell populations, myeloid lineages (macrophages, granulocytes), and DP T cells. Asterisks indicate statistically significant differences (*t*-test, $P < 0.05$). (*B*) Competitive reconstitution experiments (1:1) were performed with equal numbers of wild-type (CD45.1) and *Suv4-20h*-dn$^{vav}$ (CD45.2) bone marrow cells, which were injected into lethally irradiated mice. The ratio between the CD45.1 and CD45.2 markers was analyzed 11 mo post-transplantation in the different hematopoietic lineages. Whereas myeloid cells show significant (20%–30%) contribution of *Suv4-20h*-dn$^{vav}$ cells, <1% of the lymphoid lineages (B and T cells) are derived from *Suv4-20h*-dn$^{vav}$.

Pax5, but different from Aid, which only becomes transcribed after B-cell activation (Supplemental Fig. S11). To examine whether B-cell development is impaired in *Suv4-20h*-dn$^{vav}$ mice, we performed FACS analyses of bone marrow, spleen, and thymus cells using markers that identify progenitor, immature, and mature B cells, and also granulocytes, macrophages, and CD4$^+$, CD8$^+$ double-positive (DP) T cells. In both bone marrow and spleen of *Suv4-20h*-dn$^{vav}$ mice, there are fewer numbers of CD19$^+$ B cells as compared with wild-type controls. In particular, we observed pronounced reductions for recirculating B cells and mature B cells, but not for pro-B and pre-B cells (Fig. 7A). In addition, numbers of DP T cells in the thymus are reduced. This developmental defect appears specific to the lymphoid lineage, since numbers of myeloid cells (granulocytes and macrophages) are unaltered (Fig. 7A).

To examine whether *Suv4-20h*-dn deficiency would impair the stem cell pool of lymphoid progenitors, we conducted competitive (1:1) transplantation experiments. Equal numbers of wild-type (discriminated by the cell surface marker CD45.1) and *Suv4-20h*-dn$^{vav}$ (different CD45.2) bone marrow cells were used to repopulate the hematopoietic system of lethally irradiated wild-type mice. The well-defined fraction of multipotent progenitor cells (*lin*$^-$, *sca-1*$^+$, *c-kit*$^+$), which contains short- and long-term HSCs is slightly increased in *Suv4-20h*-dn$^{vav}$ bone marrow as compared with the wild-type control (Supplemental Fig. S12) and could therefore give rise to even higher repopulation activity. We analyzed reconstituted mice 7 wk (Supplemental Fig. S13) and 11 mo (Fig. 7) after transfer for long-term reconstitution. Intriguingly, numbers of *Suv4-20h*-dn$^{vav}$ B and T cells are severely underrepresented and amount to <1% of re-

constituted B and T cells (Fig. 7, bottom panel). In contrast, myeloid cells, such as granulocytes and macrophages, still comprised significant numbers (20%–30%) of CD45.2-positive (=*Suv4-20h*-dn) cells. This is an important control and largely excludes the possibility that *Suv4-20h*-dn HSCs would fail to repopulate the hematopoietic system because of an attenuated proliferative potential. Together, these in vivo data demonstrate an important function for the Suv4-20h enzymes to ensure the lineage program of DNA-rearranging lymphoid cells.

## Discussion

### *The control of H4K20 methylation states in mammalian chromatin*

In this study, we generated *Suv4-20h*-dn mice, which lack nearly all H4K20me2 and H4K20me3 in mammalian chromatin. Suv4-20h1 primarily induces H4K20me2, whereas Suv4-20h2 is largely responsible for H4K20me3. Surprisingly, H4K20me3 is not fully abrogated in embryonic tissues of *Suv4-20h2*$^{-/-}$ mice and readily detectable in several adult tissues (Supplemental Fig. S2). These data suggest compensatory functions of Suv4-20h1 or other HMTases. Therefore, selective loss of either H4K20me2 or H4K20me3 during mouse development cannot easily be uncoupled or independently analyzed. In *Suv4-20h*-dn mice, there is a conversion to H4K20me1 chromatin, but not to the fully unmodified state. The data demonstrate that Suv4-20h HMTases are the predominant enzymes for H4K20me2 and H4K20me3 and that H4K20me1 may be their default substrate.

The major HMTase for H4K20me1 is PrSet7, which functions in gene silencing and during mitotic chromosome condensation (Fang et al. 2002; Nishioka et al. 2002). Recent data indicate that PrSet7 generates most H4K20me1 during S phase as it localizes to replication foci and directly interacts with PCNA (Jorgensen et al. 2007; Tardat et al. 2007; Huen et al. 2008). In *Drosophila*, H4K20me1 seems to be a prerequisite to establish H4K20me2 and H4K20me3, as disruption of *PrSet7* results in the removal of all three H4K20 methylation states (Karachentsev et al. 2005). These data suggest that murine PrSet7 may also dictate H4K20 methylation in the mouse. However, probing mammalian *PrSet7* functions has been problematic, since abrogation of *PrSet7* by RNAi knockdown leads to immediate S-phase defects and a severely reduced proliferation potential (Jorgensen et al. 2007; Tardat et al. 2007). In addition, *Prset7* deficiency results in early embryonic lethality (Huen et al. 2008) and *PrSet7*-null blastocysts fail to progress beyond the four- to eight-cell stage (H. Oda and D. Reinberg, pers. comm.). Together, these observations predict that *PrSet7* function cannot be rescued by Suv4-20h enzymes. In contrast, *Suv4-20h*-dn chromatin is characterized by broad H4K20me1, which compromises, but not fully abrogates some of the biological roles of the other H4K20 methylation states. In this respect, *Suv4-20h*-dn deficiency reflects a hypomorphic mutation for H4K20 methylation.

### *H4K20 methylation and DNA damage response*

The position of Lys 20 at the boundary between the globular and flexible histone H4 domains is proposed to dominate structural transitions of chromatin (Dorigo et al. 2003; Shogren-Knaak et al. 2006). Currently, it is not known whether more rigid or more relaxed chromatin configurations could be induced by binding of proteins to the different H4K20 methylation states, although interaction of L3MBT with H4K20me1 methylated nucleosomes has been shown recently to induce nucleosome compaction in vitro (Trojer et al. 2007). We show that DNA damage repair is only partially defective in *Suv4-20h*-dn cells (Fig. 4A,B), consistent with a recent report where RNAi knockdown of Suv4-20h in mouse cells modestly reduced 53BP1 foci formation after treatment with the radio-mimetic bleomycin (Yang et al. 2008). This and earlier work (Huyen et al. 2004) suggest that 53BP1 can probably localize to chromatin at DSBs via multiple mechanisms. Although in *S. pombe* H4K20 methylation is crucial for Crb2 (a 53BP1 ortholog) localization to DSBs (Sanders et al. 2004; Du et al. 2006), Dot1-mediated H3K79 methylation has also been shown to aid 53BP1 recruitment (Huyen et al. 2004) and to contribute to DNA damage checkpoint control in *Saccharomyces cerevisiae* (Wysocki et al. 2005). Structural definition of 53BP1 binding revealed preferred interaction to H4K20me2 and, at threefold reduced affinity, also to H4K20me1 (Botuyan et al. 2006). Whereas our in vivo analysis of *Suv4-20h*-dn chromatin substantiates a role for H4K20me2 in facilitating 53BP1 recruitment, it does not exclude other targeting modes such as, e.g., H3K79 methylation.

53BP1 contains distinct domains that mediate interaction with other upstream (e.g., γH2AX) or downstream (e.g., Chk2) factors of the repair machinery and that could further stabilize 53BP1 chromatin interaction in the absence of H4K20me2. The DNA damage response has also revealed chromatin remodeling activities that precede H2A.X phosphorylation (Polo et al. 2006). No apparent defect in γH2AX foci formation was observed in *Suv4-20h*-dn cells, either after IR damage (Fig. 4A) or after laser microirradiation of euchromatic or heterochromatic subnuclear domains (data not shown). This probably excludes that H4K20me1 chromatin impairs nucleosome remodeling, although it could favor nucleosome compaction or potential cross-talk to histone H1 (Trojer et al. 2007). Interestingly, mouse cells that are triple-deficient for histone H1 isoforms (Fan et al. 2005) display more relaxed nucleosomal arrays and are more protected against DNA damage (Murga et al. 2007). Further, whereas *Suv4-20h* deficiency weakens 53BP1 association at sites of DNA damage and reflects a similar sensitivity following etoposide and hydroxyurea treatment (Fig. 4C), there are distinct stress responses between *Suv4-20h*-dn and *53BP1*-null MEFs after IR or UV exposure (Fig. 4C). These data would be consistent with Suv4-20h enzymes to participate in 53BP1-dependent and 53BP1-independent pathways, where also substrates other than histone H4 may be targeted by Suv4-20h function.

### *Control of CSR by H4K20 methylation*

Several components of the DSB repair machinery are also involved in programmed DNA rearrangements during B- and T-cell maturation. For example, *53BP1* mutant mice are severely defective in CSR; however, they do not show impaired V(D)J recombination (Manis et al. 2004; Ward et al. 2004). Conversely, several HMTases affect processing of chromatin-mediated transitions during B- and T-cell differentiation. The polycomb enzyme Ezh2 coregulates V(D)J rearrangement (Su et al. 2003), and the Suv39h1 HMTase partially controls CSR at the Cα constant region (Bradley et al. 2006). Here, we show that differentiation of B and T cells is significantly perturbed upon conditional deletion of both Suv4-20h enzymes in HSCs (Fig. 7). In addition, CSR at the Cγ1 and Cγ3 regions is decreased in *Suv4-20h*-dn$^{vav}$ B cells (Fig. 5), but there is no apparent defect in V(D)J recombination of the IgH region in pro-B cells (Supplemental Fig. S7) or of the TCRβ locus in pro-T cells (Supplemental Fig. S8).

These results could, in principle, be explained by weakened association of 53BP1 to H4K20me1 IgH chromatin, similar to the delayed recruitment at DSBs in *Suv4-20h*-dn MEFs. While this may seem plausible, we do, however, observe significantly elevated H4K20me1 levels across the Sγ1 region in both resting and activated *Suv4-20h*-dn$^{vav}$ B cells (Fig. 6A). These data argue for a more general defect in H4K20me1 chromatin. This interpretation is supported by increased translocations and deletions involving the IgH locus (Fig. 6B) and by the recent observation that *Suv4-20h*-dn MEFs display aberrant telomere length (Benetti et al. 2007). In addition, and in contrast to *53BP1*-null mice (Ward et al. 2003), *Suv4-20h*-dn mutant mice are perinatally lethal (Fig. 1B).

Further, H4K20me1 has been associated with transcriptional repression (Nishioka et al. 2002; Karachentsev et al. 2005) or activity (Papp and Muller 2006; Vakoc et al. 2006), which would predict altered gene regulation in chromatin that is severely overrepresented for H4K20me1. However, global expression profiling in mouse ES cells, and in resting and activated B cells (Supplemental Fig. S9), has indicated only very minor changes between wild-type and *Suv4-20h*-dn cells. In addition, transcriptional regulation of *53BP1* or *Aid* is not altered in the absence of Suv4-20h enzymes during distinct stages of B-cell maturation (Supplemental Fig. S11).

In summary, the cumulative data suggest a model in which *Suv4-20h* deficiency induces compromised H4K20me1 chromatin that is sensitive to DNA damage or comparable stress signals, particularly at chromosomal regions largely lacking gene activity (e.g., telomeres and centromeres) or otherwise being exposed for sequence nonspecific DNA rearrangements (e.g., CSR).

### *Functions of Suv4-20h enzymes in protecting normal development*

We have discussed H4K20me1 and H4K20me2 and how these states are altered in *Suv4-20h*-dn mice. By comparison, removal of H4K20me3 correlates with rather mild phenotypes. For H4K20 methylation, it appears that a trimethyl state is nonessential for viability, absence of a dimethyl state still allows for full fetal development (Fig. 1B), and lack of a monomethyl state is embryonic lethal (Huen et al. 2008; H. Oda and D. Reinberg, pers. comm.). H4K20me3 at pericentric heterochromatin is induced by Suv4-20h enzymes in a pathway that is dependent on preceding H3K9me3 by the Suv39h HMTases (Schotta et al. 2004). In agreement, H3K9me3 and HP1 association is maintained at pericentric hetrochromatin in the absence of the Suv4-20h HMTases (data not shown). Therefore, *Suv4-20h2*$^{-/-}$ mice show less severe defects in overall chromatin structure, genome integrity, chromosome segregation (aneuploidies), or cancer development as described for *Suv39h*-dn mice (Peters et al. 2001). However, a strong reduction of H4K20me3 has been correlated with cancer progression (Fraga et al. 2005). *H2A.X*- or *53BP1*-null mice eventually succumb to cancer development in a *p53*-dependent manner (Bassing et al. 2003; Celeste et al. 2003; Ward et al. 2005; Morales et al. 2006). Although we have not (yet) observed lymphomas in *Suv4-20h*-dn$^{vav}$ mice, it will be interesting to analyze these mutants in a *p53*-deficient background or in other accelerated tumor models.

Aberrantly high levels of H4K20me3 progressively accumulate in senescent cells or in premature aging syndromes (Shumaker et al. 2006). Furthermore, H4K20me3 levels were shown to increase with aging in mammalian tissues (Sarg et al. 2002). Future work is required to address the possible functions of the Suv4-20h enzymes in aging-associated processes and during cancer development using appropriate mouse systems. In summary, the conditional *Suv4-20h*-dn mice represent a valuable model to analyze functions of H4K20 methylation during mammalian development and clearly demonstrate the divergent biological relevance of the three distinct histone lysine methylation states.

## Materials and methods

### *Generation of conditional Suv4-20h knockout mice*

Targeting of both *Suv4-20h* genes was performed using standard technologies with details provided in the Supplemental Material.

### *Northern blots*

To analyze expression of *Suv4-20h* enzymes in embryonic development and in different tissues of adult mice, a 1.8-kb PCR DNA fragment of the Suv4-20h1 cDNA and a 1.2-kb PCR DNA fragment of the Suv4-20h2 cDNA was hybridized to multiple tissue Northern blots (BLOT2 and BLOT3; Sigma).

### *Immunofluorescence and mass-spec*

Immunofluorescence analyses were performed as described (Peters et al. 2003) using the following antibodies: H4K20me1, H4K20me2, H4K20me3 (Peters et al. 2003), 53BP1 (1:5000; Novus Biologicals), γ-H2A.X (1:2000, UBI). Five independent H4K20me2 antibodies (Peters et al. 2003; Abcam ab9052, UBI #05-672, UBI #07-747) show only low signal intensities, suggesting reduced accessibility of the H4K20me2 epitope.

For mass-spec, bulk histones from pMEFs and B cells were isolated by acid extraction and analyzed as described (Peters et al. 2003). For quantification, we used controls to ensure complete digest of the propionylated samples and synthetic peptides to correct for precolumn enrichment, HPLC separation, ionization, and mass-spectrometric detection of cleaved peptide fragments (see the Supplemental Material).

### *Proliferation, cell cycle, and DNA damage assays*

These assays were performed using standard procedures as detailed in the Supplemental Material.

### *CSR*

CSR assays with splenic B220$^+$ B cells from *Suv4-20h*-dn$^{vav}$ and age-matched wild-type mice were performed according to standard procedures as outlined in the Supplemental Material. To induce proliferation without activation of AID, B cells were stimulated with RP105 (2.5 µg/mL; BD Pharmingen). To measure GLTs and *Aid* transcripts, RNA from stimulated B cells (LPS/IL-4) was analyzed by quantitative RT–PCR.

### *ChIP*

Chromatin from resting and activated B cells from three independent wild-type and *Suv4-20h*-dn$^{vav}$ mice was prepared using standard procedures and precipitated with H4K20me1, H4K20me3, H3K9me3, H3K27me3 (Peters et al. 2003), and H3K4me3 (Abcam, ab8580) antibodies. Immunoprecipitated DNA was analyzed by quantitative PCR using primers specific for Igµ and Igγ GLT promoter and switch regions (Supplemental Table S5). Five independent antibodies against H4K20me2 (Peters et al. 2003; Abcam ab9052, UBI #05-672, UBI #07-747) failed to show significant enrichment over a no-antibody control, suggesting reduced accessibility of this epitope.

### *Competitive bone marrow reconstitution*

Lethally irradiated B6.SJL recipient mice (CD45.1) were injected with $5 \times 10^5$ bone marrow cells (1:1) derived from wild-type (CD45.1) and *Suv4-20h*-dn$^{vav}$ (CD45.2) mice. Hematopoietic lineages were analyzed by FACS as outlined in the Supplemental Material.

## Acknowledgments

We are grateful to C. Cobaleda, A. Souabni, H.C. Theussl, and H. Chen for technical assistance and helpful discussions. We thank H. Oda and D. Reinberg for allowing us to cite their work on the conditional *PrSet7* mutation in the mouse. G.S. and S.M. were supported by Marie-Curie long-term fellowships. M.T.B. is supported by NIH grant DK62248. Research in the laboratory of T.J. is sponsored by the IMP through Boehringer Ingelheim, the European Union NoE network "*The Epigenome*" (LSHG-CT-2004-503433) and the Austrian GEN-AU initiative, which is financed by funds from the Austrian Federal Ministry for Education, Science and Culture (BMBWK).

## References

Allis, C.D., Jenuwein, T., Reinberg, D., and Caparros, M.-L., ed. 2007. *Epigenetics*. Cold Spring Harbor Laboratory Press, Cold Spring Harbor, NY.

Bassing, C.H., Suh, H., Ferguson, D.O., Chua, K.F., Manis, J., Eckersdorff, M., Gleason, M., Bronson, R., Lee, C., and Alt, F.W. 2003. Histone H2AX: A dosage-dependent suppressor of oncogenic translocations and tumors. *Cell* **114:** 359–370.

Benetti, R., Gonzalo, S., Jaco, I., Schotta, G., Klatt, P., Jenuwein, T., and Blasco, M.A. 2007. Suv4-20h deficiency results in telomere elongation and derepression of telomere recombination. *J. Cell Biol.* **178:** 925–936.

Botuyan, M.V., Lee, J., Ward, I.M., Kim, J.E., Thompson, J.R., Chen, J., and Mer, G. 2006. Structural basis for the methylation state-specific recognition of histone H4-K20 by 53BP1 and Crb2 in DNA repair. *Cell* **127:** 1361–1373.

Bradley, S.P., Kaminski, D.A., Peters, A.H., Jenuwein, T., and Stavnezer, J. 2006. The histone methyltransferase Suv39h1 increases class switch recombination specifically to IgA. *J. Immunol.* **177:** 1179–1188.

Callen, E., Jankovic, M., Difilippantonio, S., Daniel, J.A., Chen, H.T., Celeste, A., Pellegrini, M., McBride, K., Wangsa, D., Bredemeyer, A.L., et al. 2007. ATM prevents the persistence and propagation of chromosome breaks in lymphocytes. *Cell* **130:** 63–75.

Celeste, A., Difilippantonio, S., Difilippantonio, M.J., Fernandez-Capetillo, O., Pilch, D.R., Sedelnikova, O.A., Eckhaus, M., Ried, T., Bonner, W.M., and Nussenzweig, A. 2003. H2AX haploinsufficiency modifies genomic stability and tumor susceptibility. *Cell* **114:** 371–383.

Delogu, A., Schebesta, A., Sun, Q., Aschenbrenner, K., Perlot, T., and Busslinger, M. 2006. Gene repression by Pax5 in B cells is essential for blood cell homeostasis and is reversed in plasma cells. *Immunity* **24:** 269–281.

Dodge, J.E., Kang, Y.K., Beppu, H., Lei, H., and Li, E. 2004. Histone H3K9 methyltransferase ESET is essential for early development. *Mol. Cell. Biol.* **24:** 2478–2486.

Dorigo, B., Schalch, T., Bystricky, K., and Richmond, T.J. 2003. Chromatin fiber folding: requirement for the histone H4 N-terminal tail. *J. Mol. Biol.* **327:** 85–96.

Du, L.L., Nakamura, T.M., and Russell, P. 2006. Histone modification-dependent and -independent pathways for recruitment of checkpoint protein Crb2 to double-strand breaks. *Genes & Dev.* **20:** 1583–1596.

Dudley, D.D., Chaudhuri, J., Bassing, C.H., and Alt, F.W. 2005. Mechanism and control of V(D)J recombination versus class switch recombination: Similarities and differences. *Adv. Immunol.* **86:** 43–112.

Fan, Y., Nikitina, T., Zhao, J., Fleury, T.J., Bhattacharyya, R., Bouhassira, E.E., Stein, A., Woodcock, C.L., and Skoultchi, A.I. 2005. Histone H1 depletion in mammals alters global chromatin structure but causes specific changes in gene regulation. *Cell* **123:** 1199–1212.

Fang, J., Feng, Q., Ketel, C.S., Wang, H., Cao, R., Xia, L., Erdjument-Bromage, H., Tempst, P., Simon, J.A., and Zhang, Y. 2002. Purification and functional characterization of SET8, a nucleosomal histone H4-lysine 20-specific methyltransferase. *Curr. Biol.* **12:** 1086–1099.

Fraga, M.F., Ballestar, E., Villar-Garea, A., Boix-Chornet, M., Espada, J., Schotta, G., Bonaldi, T., Haydon, C., Ropero, S., Petrie, K., et al. 2005. Loss of acetylation at Lys16 and trimethylation at Lys20 of histone H4 is a common hallmark of human cancer. *Nat. Genet.* **37:** 391–400.

Fuxa, M., Skok, J., Souabni, A., Salvagiotto, G., Roldan, E., and Busslinger, M. 2004. Pax5 induces V-to-DJ rearrangements and locus contraction of the immunoglobulin heavy-chain gene. *Genes & Dev.* **18:** 411–422.

Glaser, S., Schaft, J., Lubitz, S., Vintersten, K., van der Hoeven, F., Tufteland, K.R., Aasland, R., Anastassiadis, K., Ang, S.L., and Stewart, A.F. 2006. Multiple epigenetic maintenance factors implicated by the loss of Mll2 in mouse develop-

ment. *Development* **133:** 1423–1432.
Houston, S.I., McManus, K.J., Adams, M.M., Sims, J.K., Carpenter, P.B., Hendzel, M.J., and Rice, J.C. 2008. Catalytic function of the PR-Set7 histone H4 lysine 20 monomethyltransferase is essential for mitotic entry and genomic stability. *J. Biol. Chem.* doi: 10.1074/jbc.M710579200.
Huen, M.S., Sy, S.M., van Deursen, J.M., and Chen, J. 2008. Direct interaction between SET8 and proliferating cell nuclear antigen couples H4-K20 methylation with DNA replication. *J. Biol. Chem.* **283:** 11073–11077.
Huyen, Y., Zgheib, O., Ditullio Jr., R.A., Gorgoulis, V.G., Zacharatos, P., Petty, T.J., Sheston, E.A., Mellert, H.S., Stavridi, E.S., and Halazonetis, T.D. 2004. Methylated lysine 79 of histone H3 targets 53BP1 to DNA double-strand breaks. *Nature* **432:** 406–411.
Jorgensen, S., Elvers, I., Trelle, M.B., Menzel, T., Eskildsen, M., Jensen, O.N., Helleday, T., Helin, K., and Sorensen, C.S. 2007. The histone methyltransferase SET8 is required for S-phase progression. *J. Cell Biol.* **179:** 1337–1345.
Julien, E. and Herr, W. 2004. A switch in mitotic histone H4 lysine 20 methylation status is linked to M phase defects upon loss of HCF-1. *Mol. Cell* **14:** 713–725.
Karachentsev, D., Sarma, K., Reinberg, D., and Steward, R. 2005. PR-Set7-dependent methylation of histone H4 Lys 20 functions in repression of gene expression and is essential for mitosis. *Genes & Dev.* **19:** 431–435.
Kodama, S., Mori, I., Roy, K., Yang, Z., Suzuki, K., and Watanabe, M. 2001. Culture condition-dependent senescence-like growth arrest and immortalization in rodent embryo cells. *Radiat. Res.* **155:** 254–262.
Kohlmaier, A., Savarese, F., Lachner, M., Martens, J., Jenuwein, T., and Wutz, A. 2004. A chromosomal memory triggered by Xist regulates histone methylation in X inactivation. *PLoS Biol.* **2:** E171. doi: 10.1371/journal.pbio.0020171.
Lachner, M., Sengupta, R., Schotta, G., and Jenuwein, T. 2004. Trilogies of histone lysine methylation as epigenetic landmarks of the eukaryotic genome. *Cold Spring Harb. Symp. Quant. Biol.* **69:** 209–218.
Manis, J.P., Morales, J.C., Xia, Z., Kutok, J.L., Alt, F.W., and Carpenter, P.B. 2004. 53BP1 links DNA damage-response pathways to immunoglobulin heavy chain class-switch recombination. *Nat. Immunol.* **5:** 481–487.
Morales, J.C., Franco, S., Murphy, M.M., Bassing, C.H., Mills, K.D., Adams, M.M., Walsh, N.C., Manis, J.P., Rassidakis, G.Z., Alt, F.W., et al. 2006. 53BP1 and p53 synergize to suppress genomic instability and lymphomagenesis. *Proc. Natl. Acad. Sci.* **103:** 3310–3315.
Muramatsu, M., Kinoshita, K., Fagarasan, S., Yamada, S., Shinkai, Y., and Honjo, T. 2000. Class switch recombination and hypermutation require activation-induced cytidine deaminase (AID), a potential RNA editing enzyme. *Cell* **102:** 553–563.
Murga, M., Jaco, I., Fan, Y., Soria, R., Martinez-Pastor, B., Cuadrado, M., Yang, S.M., Blasco, M.A., Skoultchi, A.I., and Fernandez-Capetillo, O. 2007. Global chromatin compaction limits the strength of the DNA damage response. *J. Cell Biol.* **178:** 1101–1108.
Nishioka, K., Rice, J.C., Sarma, K., Erdjument-Bromage, H., Werner, J., Wang, Y., Chuikov, S., Valenzuela, P., Tempst, P., Steward, R., et al. 2002. PR-Set7 is a nucleosome-specific methyltransferase that modifies lysine 20 of histone H4 and is associated with silent chromatin. *Mol. Cell* **9:** 1201–1213.
O'Carroll, D., Erhardt, S., Pagani, M., Barton, S.C., Surani, M.A., and Jenuwein, T. 2001. The polycomb-group gene Ezh2 is required for early mouse development. *Mol. Cell. Biol.* **21:** 4330–4336.
Papp, B. and Muller, J. 2006. Histone trimethylation and the maintenance of transcriptional ON and OFF states by trxG and PcG proteins. *Genes & Dev.* **20:** 2041–2054.
Peters, A.H., O'Carroll, D., Scherthan, H., Mechtler, K., Sauer, S., Schofer, C., Weipoltshammer, K., Pagani, M., Lachner, M., Kohlmaier, A., et al. 2001. Loss of the Suv39h histone methyltransferases impairs mammalian heterochromatin and genome stability. *Cell* **107:** 323–337.
Peters, A.H., Kubicek, S., Mechtler, K., O'Sullivan, R.J., Derijck, A.A., Perez-Burgos, L., Kohlmaier, A., Opravil, S., Tachibana, M., Shinkai, Y., et al. 2003. Partitioning and plasticity of repressive histone methylation states in mammalian chromatin. *Mol. Cell* **12:** 1577–1589.
Polo, S.E., Roche, D., and Almouzni, G. 2006. New histone incorporation marks sites of UV repair in human cells. *Cell* **127:** 481–493.
Rice, J.C., Nishioka, K., Sarma, K., Steward, R., Reinberg, D., and Allis, C.D. 2002. Mitotic-specific methylation of histone H4 Lys 20 follows increased PR-Set7 expression and its localization to mitotic chromosomes. *Genes & Dev.* **16:** 2225–2230.
Sancar, A., Lindsey-Boltz, L.A., Unsal-Kacmaz, K., and Linn, S. 2004. Molecular mechanisms of mammalian DNA repair and the DNA damage checkpoints. *Annu. Rev. Biochem.* **73:** 39–85.
Sanders, S.L., Portoso, M., Mata, J., Bahler, J., Allshire, R.C., and Kouzarides, T. 2004. Methylation of histone H4 lysine 20 controls recruitment of Crb2 to sites of DNA damage. *Cell* **119:** 603–614.
Sarg, B., Koutzamani, E., Helliger, W., Rundquist, I., and Lindner, H.H. 2002. Postsynthetic trimethylation of histone H4 at lysine 20 in mammalian tissues is associated with aging. *J. Biol. Chem.* **277:** 39195–39201.
Schebesta, A., McManus, S., Salvagiotto, G., Delogu, A., Busslinger, G.A., and Busslinger, M. 2007. Transcription factor Pax5 activates the chromatin of key genes involved in B cell signaling, adhesion, migration, and immune function. *Immunity* **27:** 49–63.
Schotta, G., Lachner, M., Sarma, K., Ebert, A., Sengupta, R., Reuter, G., Reinberg, D., and Jenuwein, T. 2004. A silencing pathway to induce H3-K9 and H4-K20 trimethylation at constitutive heterochromatin. *Genes & Dev.* **18:** 1251–1262.
Schultz, L.B., Chehab, N.H., Malikzay, A., and Halazonetis, T.D. 2000. p53 binding protein 1 (53BP1) is an early participant in the cellular response to DNA double-strand breaks. *J. Cell Biol.* **151:** 1381–1390.
Shogren-Knaak, M., Ishii, H., Sun, J.M., Pazin, M.J., Davie, J.R., and Peterson, C.L. 2006. Histone H4-K16 acetylation controls chromatin structure and protein interactions. *Science* **311:** 844–847.
Shumaker, D.K., Dechat, T., Kohlmaier, A., Adam, S.A., Bozovsky, M.R., Erdos, M.R., Eriksson, M., Goldman, A.E., Khuon, S., Collins, F.S., et al. 2006. Mutant nuclear lamin A leads to progressive alterations of epigenetic control in premature aging. *Proc. Natl. Acad. Sci.* **103:** 8703–8708.
Su, I.H., Basavaraj, A., Krutchinsky, A.N., Hobert, O., Ullrich, A., Chait, B.T., and Tarakhovsky, A. 2003. Ezh2 controls B cell development through histone H3 methylation and IgH rearrangement. *Nat. Immunol.* **4:** 124–131.
Tachibana, M., Sugimoto, K., Nozaki, M., Ueda, J., Ohta, T., Ohki, M., Fukuda, M., Takeda, N., Niida, H., Kato, H., et al. 2002. G9a histone methyltransferase plays a dominant role in euchromatic histone H3 lysine 9 methylation and is essential for early embryogenesis. *Genes & Dev.* **16:** 1779–1791.
Tardat, M., Murr, R., Herceg, Z., Sardet, C., and Julien, E. 2007.

PR-Set7-dependent lysine methylation ensures genome replication and stability through S phase. *J. Cell Biol.* **179:** 1413–1426.

Trojer, P. and Reinberg, D. 2006. Histone lysine demethylases and their impact on epigenetics. *Cell* **125:** 213–217.

Trojer, P., Li, G., Sims III, R.J., Vaquero, A., Kalakonda, N., Boccuni, P., Lee, D., Erdjument-Bromage, H., Tempst, P., Nimer, S.D., et al. 2007. L3MBTL1, a histone-methylation-dependent chromatin lock. *Cell* **129:** 915–928.

Vakoc, C.R., Sachdeva, M.M., Wang, H., and Blobel, G.A. 2006. Profile of histone lysine methylation across transcribed mammalian chromatin. *Mol. Cell. Biol.* **26:** 9185–9195.

Ward, I.M., Minn, K., van Deursen, J., and Chen, J. 2003. p53 Binding protein 53BP1 is required for DNA damage responses and tumor suppression in mice. *Mol. Cell. Biol.* **23:** 2556–2563.

Ward, I.M., Reina-San-Martin, B., Olaru, A., Minn, K., Tamada, K., Lau, J.S., Cascalho, M., Chen, L., Nussenzweig, A., Livak, F., et al. 2004. 53BP1 is required for class switch recombination. *J. Cell Biol.* **165:** 459–464.

Ward, I.M., Difilippantonio, S., Minn, K., Mueller, M.D., Molina, J.R., Yu, X., Frisk, C.S., Ried, T., Nussenzweig, A., and Chen, J. 2005. 53BP1 cooperates with p53 and functions as a haploinsufficient tumor suppressor in mice. *Mol. Cell. Biol.* **25:** 10079–10086.

Wysocki, R., Javaheri, A., Allard, S., Sha, F., Cote, J., and Kron, S.J. 2005. Role of Dot1-dependent histone H3 methylation in G1 and S phase DNA damage checkpoint functions of Rad9. *Mol. Cell. Biol.* **25:** 8430–8443.

Yang, H., Pesavento, J.J., Starnes, T.W., Cryderman, D.E., Wallrath, L.L., Kelleher, N.L., and Mizzen, C.A. 2008. Preferential dimethylation of histone H4 lysine 20 by Suv4-20. *J. Biol. Chem.* **283:** 12085–12092.